Materials Research Bulletin 205 (2027) 114397

Contents lists available at ScienceDirect

Materials Research Bulletin

journal homepage: www.elsevier.com/locate/matresbu

Research papers

Liquid metal–integrated polyimide nanofibers for high-temperature triboelectric energy harvesting

Peng Wu [a], Kamyar Shirvanimoghaddam [b,*], İlhan Özen [c], Nauman Ali Choudhry [b], Agnieszka Kooijman [d], Prasaanth Ravi Anusuyadevi [d], Peyman Taheri [d], Minoo Naebe [a,*]

[a] Institute for Frontier Materials, Deakin University, Waurn Ponds, Victoria 3216, Australia
[b] School of Fashion and Textiles, RMIT University, Brunswick, Victoria 3056, Australia
[c] Department of Textile Engineering, Faculty of Engineering, Erciyes University, Melikgazi, Kayseri, Turkey
[d] Department of Materials Science and Engineering, Faculty of Mechanical Engineering, Delft University of Technology, Delft 2628 CD, the Netherlands

ARTICLE INFO

Keywords:
Triboelectric nanogenerators
Polyimide nanofibers
Liquid metal nanospheres
High-temperature triboelectrics
Self-powered sensors

ABSTRACT

Triboelectric nanogenerators (TENGs) capable of operating at elevated temperatures remain constrained by charge dissipation and the poor thermal stability of conventional polymer dielectrics. Here, liquid metal (LM)-integrated polyimide (PI) nanofibers are developed as a thermally robust triboelectric platform for harsh-environment energy harvesting. Gallium-based LM nanospheres are incorporated into electrospun PI nanofibers through a sonication-assisted dispersion strategy, producing uniform composite membranes while preserving the fibrous architecture. Structural and surface analyses reveal that LM incorporation drastically modulates the local electrostatic environment of the fibers, consistent with enhanced interfacial polarization and charge trapping. Among the investigated formulations, the membrane containing 5 wt% LM delivers the optimal ambient triboelectric output, achieving an open-circuit voltage (V_{oc}) of 8.40 V, improved capacitor charging behavior, and stable operation over 10,000 cycles. Under elevated-temperature testing, the output exhibited a positive temperature dependence, reaching a maximum V_{oc} of 11.76 V at 200 °C before declining at higher temperatures, while measurable output was sustained up to 300 °C.

1. Introduction

Triboelectric nanogenerators (TENGs) have emerged as an effective platform for harvesting distributed mechanical energy and powering self-sustained sensors owing to their lightweight structures, diverse material choices, and simple device architectures [1,2]. In parallel, electrospun nanofibrous dielectrics have attracted increasing interest in TENG design because their high surface area, tuneable porosity, and controllable morphology can promote charge generation, interfacial polarization, and device flexibility [3]. These features make electrospun nanofiber membranes particularly attractive for wearable and structural energy harvesters, where both conformability and output stability are important. To tackle environmental energy losses, recent leading attempts have leveraged electrospun hierarchical nanofibrous networks encapsulated with functional multi-fillers to synergistically mitigate charge dissipation and stabilize voltage outputs under fluctuating ambients [4]. Concurrently, the strategic integration of fibers or functional additives to reinforce composite matrices has been widely recognized as a versatile paradigm to optimize flexural behaviors, structural longevity, and operational stability across various modern engineering and sustainable applications [5–8].

Despite these advantages, operating polymer-based TENGs at elevated temperatures remains a major challenge. At high temperatures, thermionic emission, charge dissipation, and thermally induced structural changes can markedly reduce surface charge retention and weaken electrical output. To mitigate this thermal charge decay and structural degradation, recent pioneering works have attempted to enhance the intrinsic thermal oxidation resistance of advanced matrices (such as liquid crystalline polymers) via functional antioxidant stabilizers, achieving a distinct high-temperature output enhancement [9]. Additionally, constructing robust organic/inorganic networks—such as integrating aramid nanofibers (ANFs) with ferroelectric nanoparticles—has emerged as an effective paradigm to explicitly suppress hot electron emission and sustain structural integrity under thermal stress [10]. Recent studies have therefore focused on high-temperature-operable triboelectric materials and device

* Corresponding authors.
E-mail addresses: Kamyar.shirvani.moghaddam@rmit.edu.au (K. Shirvanimoghaddam), minoo.naebe@deakin.edu.au (M. Naebe).

https://doi.org/10.1016/j.materresbull.2026.114397
Received 19 May 2026; Received in revised form 12 August 2026; Accepted 13 August 2026
Available online 15 August 2026

configurations [11,12]. In this context, polyimide (PI) is one of the most promising dielectric candidates due to its excellent thermal resistance, chemical stability, and mechanical integrity. Electrospun PI nanofiber TENGs have already demonstrated the ability to harvest energy at elevated temperatures [13], and subsequent work has shown that the temperature dependence of PI-based triboelectric output is governed by a complex balance between thermally enhanced polarization and temperature-induced charge loss [14]. These studies clearly establish PI as a robust high-temperature triboelectric platform, but they also show that further materials engineering is needed to raise output while preserving thermal stability.

A promising strategy for improving triboelectric dielectrics is the incorporation of liquid-metal (LM) micro- or nano-inclusions. Gallium-based liquid metals such as Galinstan offer unusual combinations of metallic conductivity, deformability, low volatility, and interfacial responsiveness, making them appealing functional fillers for soft energy systems [15]. As comprehensively reviewed recently, while the fluidic nature and adaptable oxide shell of LMs offer vast design pathways for macromolecular composites, challenges regarding their long-term surface stability and interfacial compliance within polymer matrices must be addressed to unlock their full potential in reliable flexible electronics [16]. In triboelectric composites, LM droplets or nano-capsules can introduce abundant internal interfaces, enhance interfacial polarization, and increase charge-storage capability when they are well dispersed within the polymer matrix [17]. For instance, constructing core–shell structured liquid metal nanocapsules via surface engineering has been demonstrated to effectively resolve interfacial mismatch while providing dense interfacial polarization sites to drastically boost triboelectric power density [18]. Recent studies have shown that LM incorporation can substantially improve triboelectric output in polymer systems such as PVDF-HFP nanofiber membranes [19] and surface-modified LM nano-capsule/polymer composites [20]. At the same time, the performance gain strongly depends on dispersion state, loading level, and matrix compatibility; excessive aggregation can instead reduce effective electrification and destabilize the composite structure [21].

These considerations make LM–PI composites particularly interesting for high-temperature triboelectric applications. PI provides the thermal and structural backbone required for elevated-temperature operation, while LM nanospheres may enhance dielectric response through interfacial polarization and localized charge trapping. However, unlike low-temperature flexible TENG systems, LM addition to PI for elevated-temperature energy harvesting may also introduce competing effects. Although dispersed LM inclusions can strengthen dielectric behaviour, their high thermal conductivity and possible aggregation at higher loading may accelerate heat transfer, alter local charge distribution, and weaken triboelectric performance under harsh thermal conditions[22]. As a result, the key question is not simply whether LM improves PI, but how LM loading and dispersion regulate the trade-off between enhanced dielectric response and temperature-dependent charge loss in a thermally stable nanofibrous matrix.

In this work, we develop liquid metal–integrated polyimide nanofibers and investigate their suitability as high-temperature triboelectric materials. Galinstan nanospheres were incorporated into electrospun PI nanofibers through a dispersion-assisted approach, and the effects of LM concentration on morphology, chemical structure, thermal behaviour, and triboelectric output were systematically examined. Particular attention was given to identifying the optimum loading level and understanding the structure–property relationships governing voltage output, capacitor charging, durability, elevated-temperature response and electrostatic/interface modification to achieve a balance between triboelectric functionality and wide-temperature operability. By combining morphological and thermal characterization with triboelectric performance analysis, this study aims to clarify how LM nano-inclusions modify PI nanofiber behaviour and to establish a practical route toward thermally robust, high-performance triboelectric nanofiber composite membranes for advanced energy-harvesting applications. The objective of this work is not to maximize the absolute electrical output, but to develop a thermally robust triboelectric platform capable of stable operation under elevated temperatures.

2. Experimental

2.1. Materials

The polyimide amid acid (PAA) was prepared by the monomer 4,4′-Oxydiphthalic anhydride (ODPA) and p-Phenylenediamine (PDA) as the precursor for PI. N,N-Dimethylformamide (DMF) was used as the solvent without further purification. A gallium-based liquid metal alloy (Galinstan; composed of Ga-In-Sn) was used as the conductive filler material. All of the chemicals were purchased from Sigma-Aldrich (Sydney, Australia).

2.2. Preparation of liquid metal nanospheres

Liquid metal (LM) nanospheres were prepared via a sonication-assisted dispersion method. A predetermined amount of bulk Galinstan and poly(vinyl pyrrolidone) (PVP) were added to DMF, and subjected to probe ultrasonication (50% amplitude, 450 W) for a fixed duration (10 mins) under ambient conditions (20°C temperature and 65% relative humidity). High-energy acoustic waves generated during sonication induce cavitation and hydrodynamic shear forces, leading to the formation of nanoscale LM droplets. These droplets are stabilized by a thin native oxide layer (Ga_2O_3), which prevents coalescence and facilitates uniform dispersion within the polymer matrix. The resulting LM nanosphere dispersion was used immediately for composite dope preparation to minimise re-agglomeration.

2.3. Fabrication of PI/LM composite nanofibers

PI/LM composite nanofibers were fabricated via electrospinning. The PAA dope was prepared in DMF to obtain a homogeneous spinning solution. 1.55 mL of LM nanosphere dopes with concentrations of 14, 70, and 140 mg/mL (using PVP as a stabilizer) were added to 10 mL of 18 wt% PAA dope. Mixed PAA/LM dopes with varying weight fractions (1, 5, and 10 wt%) were obtained through continuous shaking followed by Vortex Shaker to ensure uniform dispersion.

The resulting mixture was loaded into a syringe and electrospun under controlled conditions (applied voltage: 18 kV, flow rate: 0.6 mL h^{-1}, tip-to-collector distance: 18 cm). The nanofibers were collected on a grounded aluminium foil.

The PAA/LM nanofiber membranes were subsequently imidized in an oven according to the following procedure: 100 ℃ for 1 h, 200 ℃ for 1 h, and 300 ℃ for 1 h.

2.4. Device fabrication

The Single-Electrode Mode (SE-TENG) was adopted in this work. Triboelectric nanogenerator (TENG) devices were fabricated using the electrospun PI/LM nanofiber membranes as the dielectric layer. The nanofiber mat was attached to a conductive electrode (aluminium foils), which served as the ground electrode.

A counter triboelectric layer (steel tapping head) was used to form a vertical SE-TENG configuration. Electrical connections were established using conductive wires, and the device was assembled to ensure consistent contact and separation during operation.

2.5. Characterisation

2.5.1. Morphological and structural analysis

The morphology and fiber structure of the electrospun nanofiber membranes were examined using scanning electron microscopy (SEM).

Fiber diameter distribution and surface morphological features were analysed using image processing software.

Atomic force microscopy (AFM) and Kelvin probe force microscopy (KPFM) were employed to investigate the nanoscale surface topography and local surface potential distribution of the pristine PI and PI/LM nanofiber membranes, respectively. Prior to analysis, the nanofiber samples were dispersed in ethanol and sonicated in an ultrasonic bath for 10 min to obtain a homogeneous suspension. The resulting suspension was drop-cast onto aluminium foil substrates and dried under ambient conditions before characterization.

AFM and KPFM measurements were conducted using a Dimension Edge atomic force microscope (Bruker, USA). Surface topography images were collected during the forward scan in tapping mode, whereas the surface potential/contact potential difference (CPD) measurements were obtained during the backward scan using KPFM mode. During surface potential acquisition, the probe tip was lifted approximately 300 nm above the sample surface to minimise topographic interference with the surface potential signal.

All measurements were performed over a scan area of $10 \times 10\ \mu m^2$ with an image resolution of 256×256 pixels and a scan rate of $20\ \mu m\ s^{-1}$. A conductive silicon probe (SCM-PIT-V2, Bruker) with an approximate tip radius of 25 nm was used for both AFM and KPFM measurements. The probe consisted of an antimony-doped silicon cantilever coated with Pt-Ir on the backside to enhance conductivity and improve surface potential sensitivity.

The obtained AFM topography images and KPFM surface potential maps were processed and analysed using Gwyddion software. These analyses were used to evaluate the influence of liquid metal (LM) incorporation on surface morphology, nanoscale roughness, and local electrostatic behaviour.

2.5.2. Thermal analysis

Thermal stability of the nanofiber membranes was evaluated using thermogravimetric analysis (TGA) under a nitrogen atmosphere. The decomposition behaviour and residual weight were analysed to assess the effect of LM incorporation on thermal performance.

2.5.3. Electrical and triboelectric performance

The electrical output performance of the TENG devices was evaluated under periodic mechanical excitation using a customized tapping device with a compression force of 10 N at working areas of 4 cm^2, displacement of 2 mm, and a frequency of 2 Hz. Open-circuit voltage (Voc), short-circuit current (Isc), and transferred charge were recorded using an oscilloscope (Rohde & Schwarz, RTM3004). To ensure data reliability and eliminate localized operational fluctuations, the reported output voltage values were obtained by calculating the statistical mean of peak-to-peak values across 20 consecutive contact–separation cycles under a continuous 2 Hz operating frequency. The corresponding standard deviations were calculated to quantify cycle-to-cycle variability.

Capacitor charging experiments were performed to assess the practical energy storage capability of the devices. Different capacitors (47 μF) were charged using the TENG output, and the voltage evolution was monitored.

2.5.4. High-temperature performance testing

To evaluate thermal robustness, the TENG devices were tested at elevated temperatures using a controlled heating stage. The output performance was recorded at different temperatures (room temperature to 300 °C), and the variation in electrical output was analysed.

Durability and stability tests were conducted under repeated operation cycles and thermal exposure to assess long-term device reliability.

3. Results and discussion

3.1. Morphology, fiber structure, and LM nanosphere dispersion

The successful incorporation and dispersion of liquid metal (LM) nanospheres within electrospun polyimide (PI) nanofibers are critical for achieving enhanced triboelectric performance, as filler distribution strongly influences dielectric polarization, charge trapping, and structural uniformity. Gallium-based liquid metals possess high surface tension and naturally tend to coalesce into larger droplets; therefore, controlled droplet size reduction and stabilization are essential prior to electrospinning. In the present work, a sonication-assisted dispersion strategy combined with poly(vinyl pyrrolidone) (PVP) as a stabilizing agent was employed to generate uniformly dispersed LM nanospheres. High-energy acoustic waves generated during sonication induce cavitation and hydrodynamic shear forces, leading to the breakup of bulk LM into nanoscale droplets, while the formation of a thin native oxide shell suppresses recoalescence and improves colloidal stability. Similar sonochemical approaches have previously been reported for the preparation of stable gallium-based LM nanoparticles for composite systems [23].

The qualitative optimization process used to obtain a stable LM suspension is illustrated in Fig. 1, which shows the progressive effect of increasing PVP concentration and repeated sonication cycles (50% amplitude, 450 W, and 10 mins/cycle) on dispersion behaviour. At low surfactant content, visible settling of LM droplets was observed, whereas improved stability was achieved only when sufficient PVP loading was combined with repeated sonication. These observations indicate that both steric stabilization and adequate mechanical energy input are required to overcome the intrinsic coalescence tendency of LM droplets and produce a homogeneous precursor suitable for electrospinning. Table 1 shows the details and observations of LM dispersions states.

The morphology of the electrospun PI/LM nanofiber membranes was examined using scanning electron microscopy (SEM). As shown in Fig. 2a-f, the membranes consisted of a continuous nonwoven network of randomly oriented fibers with smooth surfaces and no obvious bead defects or fiber fusion, indicating that the addition of LM nanospheres did not destabilize the electrospinning process. At higher magnification, localized spherical protrusions were visible along selected fibers, suggesting the presence of embedded or partially encapsulated LM domains retained within the PI matrix during jet stretching and solvent evaporation. It is worth noting that while fewer larger LM particles are observable on the fiber surfaces via SEM, a substantial number of smaller, nanoscale LM droplets are completely encapsulated inside the core of the PI nanofibers. This internal embedding configuration, firmly validated by subsequent TEM analysis, effectively preserves the initial porous architecture of pristine PI while providing abundant nested hetero-interfaces for polarization enhancement.

The fiber diameter distribution of the PI/LM membrane containing 5 wt% LM is presented in Fig. 2g. The fibers exhibited a mean diameter of 159.27 nm, with a measured range of 73.52–326.49 nm. This nanoscale fibrous structure provides a high specific surface area and abundant contact-active sites, both of which are beneficial for triboelectric charge generation. The relatively broad distribution is typical of electrospun systems and may reflect local viscosity variation or filler-induced changes in jet elongation behaviour.

Transmission electron microscopy (TEM) provided direct evidence for the successful incorporation of LM nanospheres inside the nanofibers. As shown in Fig. 3, distinct high-contrast spherical inclusions were observed within the fiber body, consistent with the presence of electron-dense LM domains encapsulated by the PI matrix. This embedded morphology is advantageous because it enables LM to modify the dielectric microenvironment without forming a continuous conductive pathway that could short-circuit the triboelectric layer. Instead, isolated inclusions are expected to promote interfacial polarization and localized charge storage under repeated contact-separation

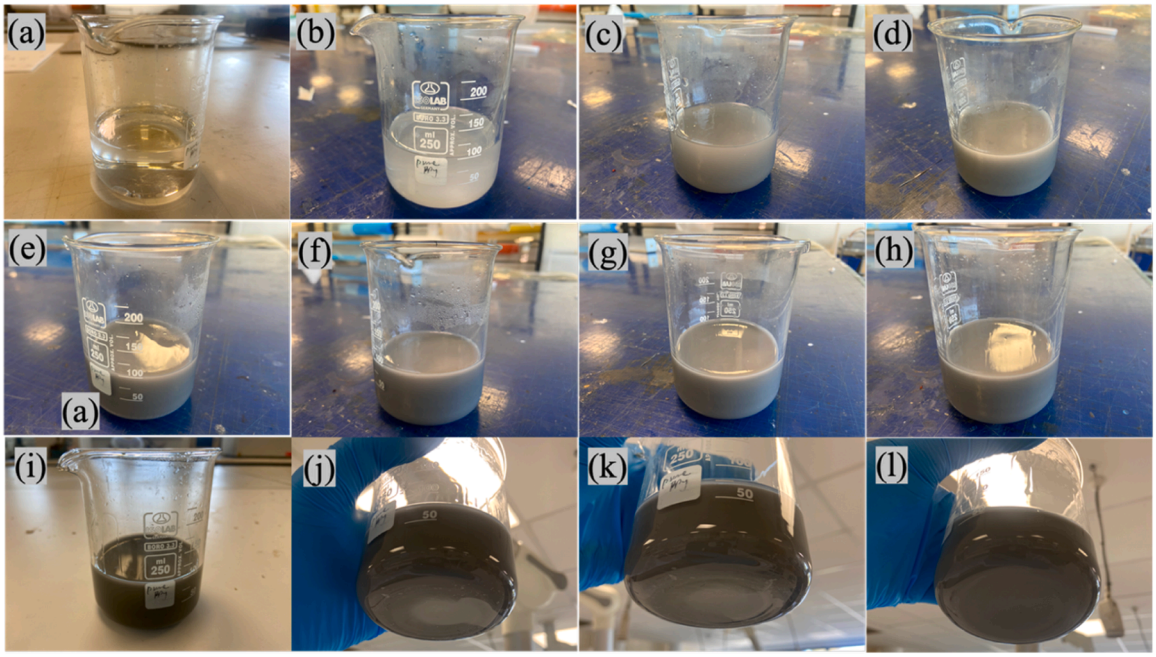

Fig. 1. Photographic sequence showing optimization of LM (500 mg) dispersion under varying PVP concentrations and sonication cycles(a-l).

Table 1
Observations of LM (500 mg) dispersion with increasing PVP amounts and sonication cycles.

Sample	Sonication Cycle	PVP Amount (mg)	Observations
a	No sonication	400	Initial state; LM not dispersed.
b	1st sonication	400	Partial dispersion observed; LM still settling.
c	2nd sonication	400	Dispersion improved, although complete stabilization was not achieved.
d	3rd sonication	400	Similar behaviour to the 2nd cycle; visible LM particles remained.
e	4th sonication	400	Further dispersion achieved; however, LM settling was still observed.
f	5th sonication	600	Improved dispersion with reduced settling behaviour.
g	6th sonication	800	More uniform dispersion obtained; minor visible LM particles remained.
h	6th sonication	1000	Further improvement in dispersion with partial settling.
i	6th sonication	1200	Significant improvement achieved with only minor settling observed.
j	6th sonication	1400	Near-complete dispersion with minimal particle agglomeration.
k	6th sonication	1600	Almost fully dispersed system with only trace visible particles.
l	7th sonication	1600	Complete and stable LM dispersion achieved.

motion.

To further investigate nanoscale surface characteristics, atomic force microscopy (AFM) and Kelvin probe force microscopy (KPFM) were conducted on pristine PI fibers and LM-containing fibers. The AFM topography images of pristine PI fibers (Fig. 4a,b) and PI/LM fibers (Fig. 4d,e) show that both samples retained comparable fibrous surface architecture, confirming that LM incorporation did not disrupt the fundamental nanofiber morphology. However, the PI/LM sample exhibited more pronounced local height variations, which are consistent with subsurface or partially exposed LM inclusions generating localized surface undulations. Such morphological heterogeneity may improve microscale contact intimacy during triboelectric cycling.

The KPFM surface potential maps (Fig. 4c,f) revealed clear differences in the electrostatic landscape of the two materials. The pristine PI fibers exhibited relatively uniform surface potentials centred around 0.6 V, whereas the PI/LM fibers showed an increased average surface potential of 0.8 V, with localized regions approaching 0.8 - 1.0 V. The elevated and spatially heterogeneous surface potential **suggests** that LM incorporation **may** modifies the electronic surface environment of the nanofiber membrane. This behaviour is consistent with the possible presence of enhanced charge trapping and interfacial polarization arising from the dielectric mismatch between PI and dispersed LM inclusions, which may contribute to contribute positively to triboelectric output performance.

Experimentally, these results demonstrate successful LM incorporation, while the observed changes in surface morphology and electrostatic potential suggest that LM nanospheres may modify the local dielectric environment, which may contribute to enhanced triboelectric charge generation. (The full detail of the KPFM characterisation is provided in Supplementary data) However, it should be noted that while the enhanced surface potential confirmed by KPFM offers strong evidence of a modified local electrostatic environment, it does not establish a direct quantitative link to the macro-scale dynamic triboelectric charge density. Fully decoupling the individual contributions of Maxwell-Wagner interfacial polarization from deeper defect-induced charge trapping remains a challenge under the current setup. To establish a more quantitative correlation and track charge storage lifetimes, complementary methodologies such as surface charge decay measurements and broadband dielectric spectroscopy will be essential. This limitation represents a crucial target for our future investigations to further refine the macro-micro theoretical models of liquid metal-based dielectrics.

3.2. *Triboelectric output performance at ambient conditions*

The triboelectric output performance of the electrospun PI/LM nanofiber membranes was first evaluated under ambient conditions to determine the influence of liquid metal (LM) incorporation on electrical energy harvesting behaviour. Open-circuit voltage (Voc) measurements

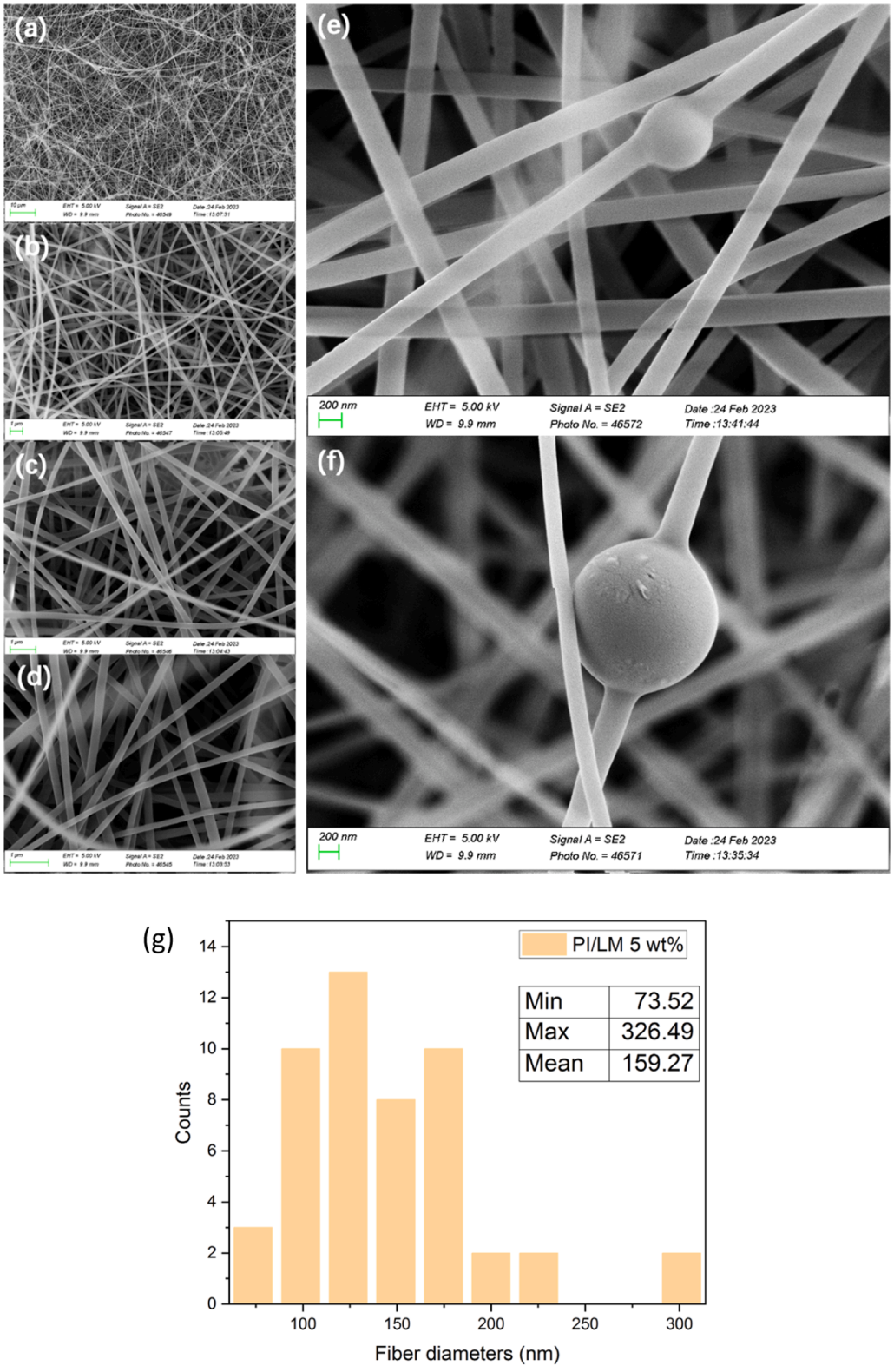

Fig. 2. SEM images of PI/LM nanofibers at different magnifications showing fiber network morphology and representative spherical LM nodules (a-f), together with fiber diameter distribution histogram for the 5 wt% LM sample (g).

for pristine PI and PI/LM nanofibers with different LM loadings are presented in Fig. 5a. The pristine PI nanofiber membrane exhibited the lowest output voltage of 3.56±0.08 V, whereas all LM-containing samples showed a clear improvement in triboelectric response. Among the investigated compositions, the 5 wt% LM sample delivered the highest Voc of 8.40±0.42 V, representing an increase of approximately 136% relative to pristine PI. In comparison, the 1 wt% LM and 10 wt% LM samples generated Voc values of 5.84±0.28 V and 6.16±0.53 V, respectively.

The substantial increase in output after LM incorporation indicates

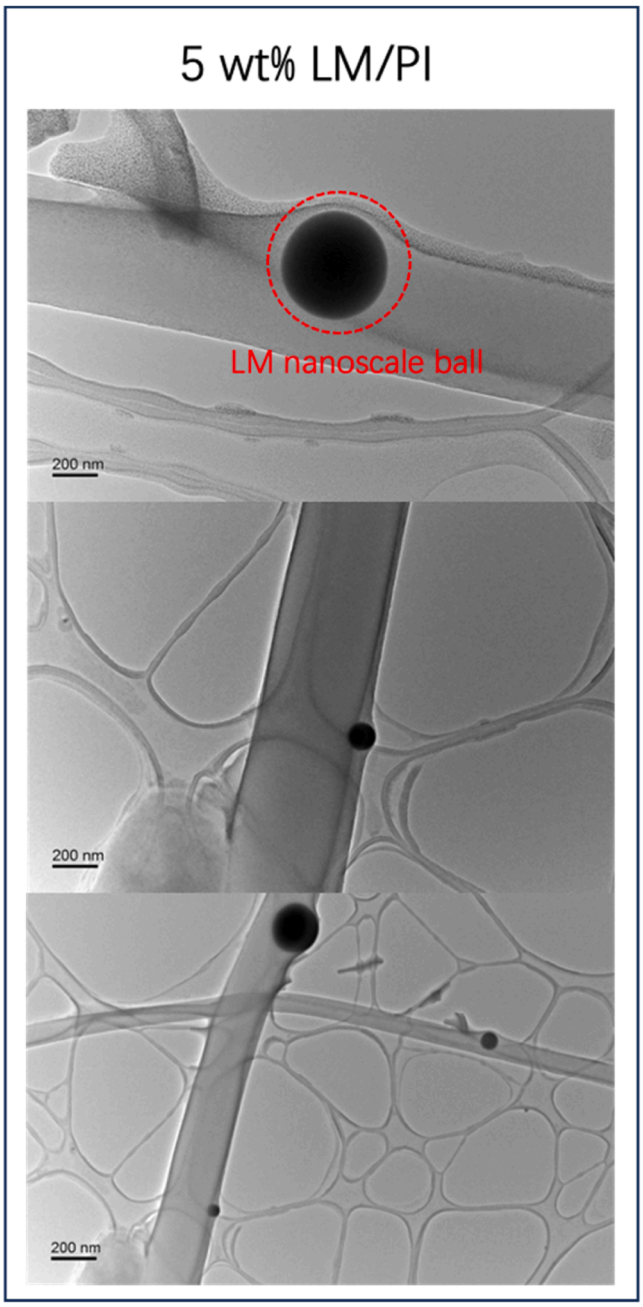

Fig. 3. TEM images of PI/LM nanofibers showing embedded LM nanospheres within the PI fiber structure.

that dispersed LM nanospheres **may** modify the dielectric characteristics of the PI nanofiber matrix. Under repeated contact-separation motion, isolated LM inclusions are proposed to enhance interfacial polarization and **may** increase local charge storage capacity, thereby promoting higher charge transfer and voltage generation. However, the dependence of performance on LM loading demonstrates that the relationship is non-linear, with an optimum concentration required to maximize the beneficial dielectric effect while maintaining structural and electrical uniformity.

Practical energy storage capability was further assessed through capacitor charging experiments using a 47 μF capacitor, as shown in Fig. 5b. Consistent with the Voc results, the 5 wt% LM membrane exhibited the most rapid charging behaviour, reaching approximately 1.8 V within 100 s. The 1 wt% LM and 10 wt% LM samples displayed intermediate charging rates, while pristine PI showed the slowest voltage accumulation. These results confirm that the enhanced triboelectric output of the optimised PI/LM membrane can be effectively converted into stored electrical energy, highlighting its practical potential for low-power self-powered systems.

The superior charging behaviour of the 5 wt% LM sample can be attributed not only to higher instantaneous voltage generation, but also to improved charge collection efficiency arising from favourable dielectric contrast and more effective retention of triboelectrically generated charges. In contrast, the lower output of pristine PI reflects the limited polarization capability of the neat polymer matrix, while the reduced performance at excessive LM loading suggests the onset of filler aggregation or partial conductive screening effects, which may hinder effective charge separation.

The ambient-condition results demonstrate that controlled incorporation of LM nanospheres significantly improves the energy harvesting capability of PI nanofiber membranes, with 5 wt% LM identified as the optimum composition among the investigated formulations. This optimum behaviour is examined in greater detail through mechanistic and durability analyses in the following section.

3.3. Effect of LM loading on triboelectric performance: mechanistic interpretation and operational stability

The ambient-condition performance results revealed a clear dependence of triboelectric output on liquid metal (LM) loading, with the 5 wt % LM sample exhibiting the highest open-circuit voltage and fastest capacitor charging behaviour among the investigated formulations. This concentration-dependent trend indicates that the enhancement mechanism is governed by a balance between beneficial dielectric effects at moderate LM loading and adverse structural or electrical effects at excessive filler content.

At relatively low loading (1 wt% LM), the number of dispersed LM nanospheres within the PI matrix is limited, which likely restricts the extent of interfacial polarization and charge-storage enhancement that can be introduced into the dielectric layer. Although the presence of LM still improves output compared with pristine PI, the concentration is insufficient to maximize the available filler–matrix interfacial area required for stronger triboelectric enhancement.

When the LM content was increased to 5 wt%, a substantial improvement in output performance was achieved. Under a same sonication process across all samples, this intermediate loading allows the sub-micron and nanoscale LM droplets to remain sufficiently isolated and uniformly distributed throughout the nanofiber matrix, as supported by the morphological observations in Section 3.1. Analogous to the high-density heterogeneous interfaces and structural defects produced via multi-phase hybridization or localized domain evolution that dramatically enhance local polarization and transport attenuation characteristics [24,25]. Such a dispersed configuration is proposed to create abundant heterogeneous interfaces between PI and LM domains, promoting Maxwell-Wagner-type interfacial polarization, localized charge trapping, and improved dielectric response under repeated contact–separation motion. In addition, the increased surface potential observed in the KPFM analysis suggests that LM incorporation modifies the local electrostatic environment in a manner favourable for charge generation and retention. These mechanisms may collectively explain the superior performance of the 5 wt% LM membrane.

Further increasing the LM content to 10 wt% resulted in a reduction in output relative to the optimum composition, despite still outperforming pristine PI. This decline suggests that excessive filler loading may compromise the beneficial dispersion state achieved at lower concentrations. At higher LM content, closer particle proximity or partial agglomeration may reduce the effective interfacial area available for polarization. Furthermore, according to the continuous conductive network and impedance matching theories in flexible electronics[26, 27], such overcrowded metallic domains may deteriorate the surface impedance balance. **It may** generate localized conductive pathways, or

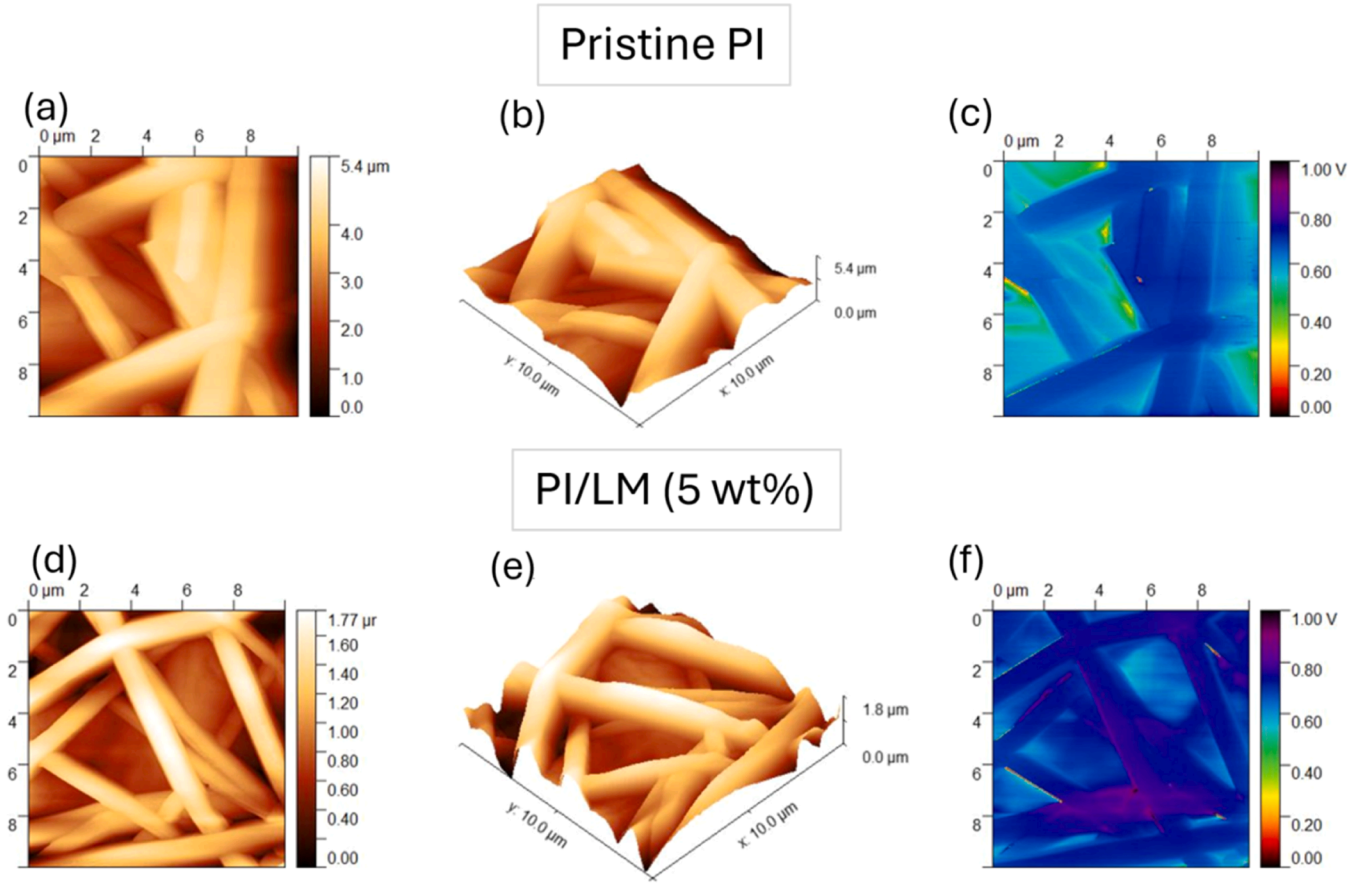

Fig. 4. AFM topography and KPFM surface potential maps of pristine PI and PI/LM nanofibers. (a) 2D AFM topography, (b) 3D AFM topography, and (c) KPFM surface potential map of pristine PI fibers; (d) 2D AFM topography, (e) 3D AFM topography, and (f) KPFM surface potential map of PI/LM fibers.

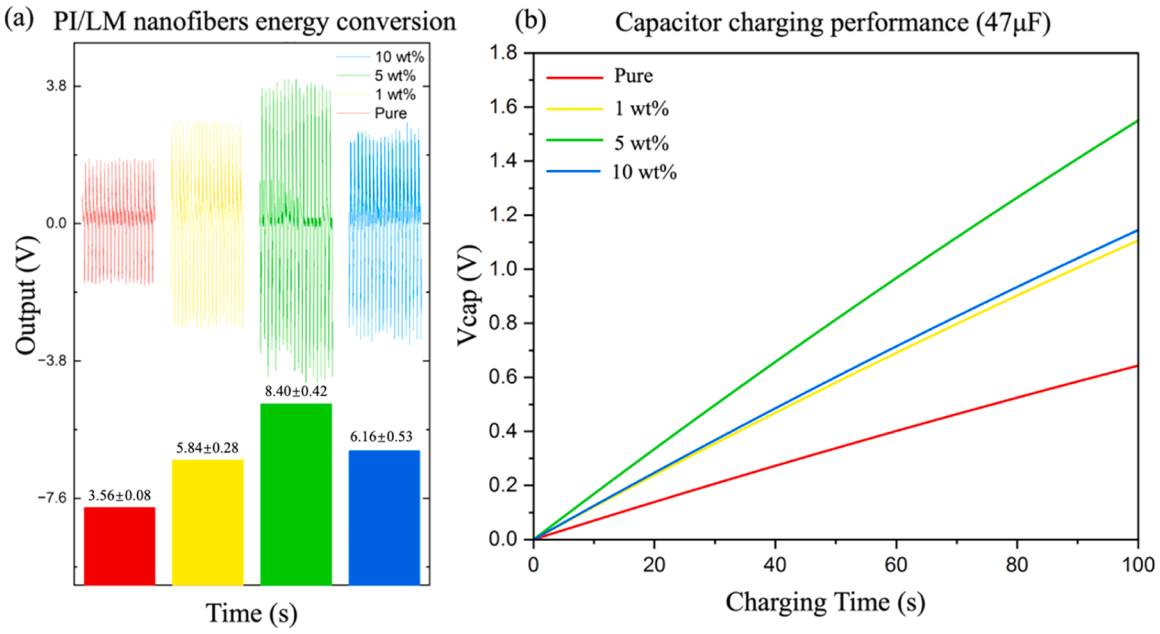

Fig. 5. Triboelectric output performance of pristine PI and PI/LM nanofibers under ambient conditions: (a) open-circuit voltage (Voc) for different LM loadings (0, 1, 5, and 10 wt%), and (b) capacitor charging profiles of a 47 μF capacitor over 100 s.

partially screen surface charges, thereby suppressing efficient triboelectric charge separation. In electrospun systems, excessive filler loading may also alter solution rheology and local fiber uniformity, further contributing to reduced output performance.

The operational durability of the optimised membrane was evaluated through continuous cycling at 2.5 Hz over 10,000 cycles. As shown in

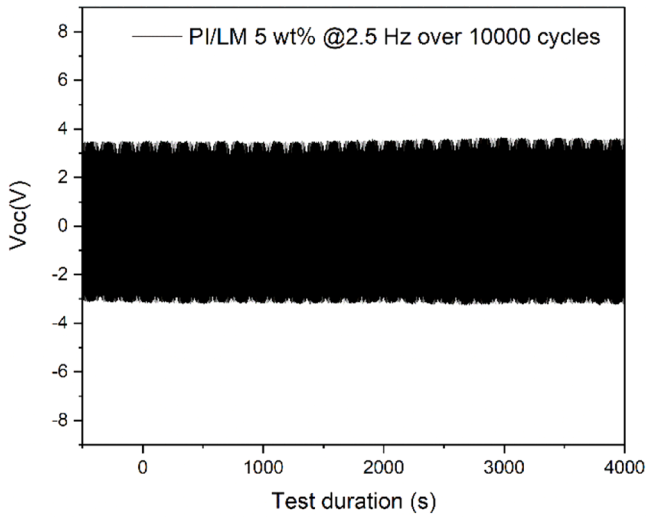

Fig. 6. Long-term mechanical durability test of the PI/LM 5 wt% composite membrane at 2.5 Hz over 4000 s (over 10,000 continuous contact–separation cycles), demonstrating excellent output retention.

Fig. 6, the 5 wt% LM nanofiber membrane maintained a stable and repeatable voltage output throughout the test period, with no obvious signal degradation. The retained performance demonstrates that LM incorporation at the optimum loading does not undermine the structural integrity of the fibrous membrane during repeated mechanical deformation. Instead, the stable response suggests that the dispersed LM domains remained effectively immobilized within the PI matrix, preserving the dielectric and interfacial characteristics responsible for enhanced triboelectric output.

The excellent cycling stability is particularly important for practical self-powered devices, where long-term mechanical reliability is essential. The combination of improved output and sustained durability indicates that moderate LM incorporation provides a favourable route for enhancing triboelectric performance without sacrificing operational robustness.

Accordingly, 5 wt% LM was identified as the optimum composition among the investigated formulations, where interfacial polarization enhancement, structural uniformity, and charge stability were most favourably balanced. This composition was therefore selected for subsequent thermal and elevated-temperature performance evaluation.

3.4. *Thermal stability of PI/LM nanofibers*

The thermal behaviour of the PI/LM nanofiber membranes was investigated to determine whether incorporation of liquid metal (LM)

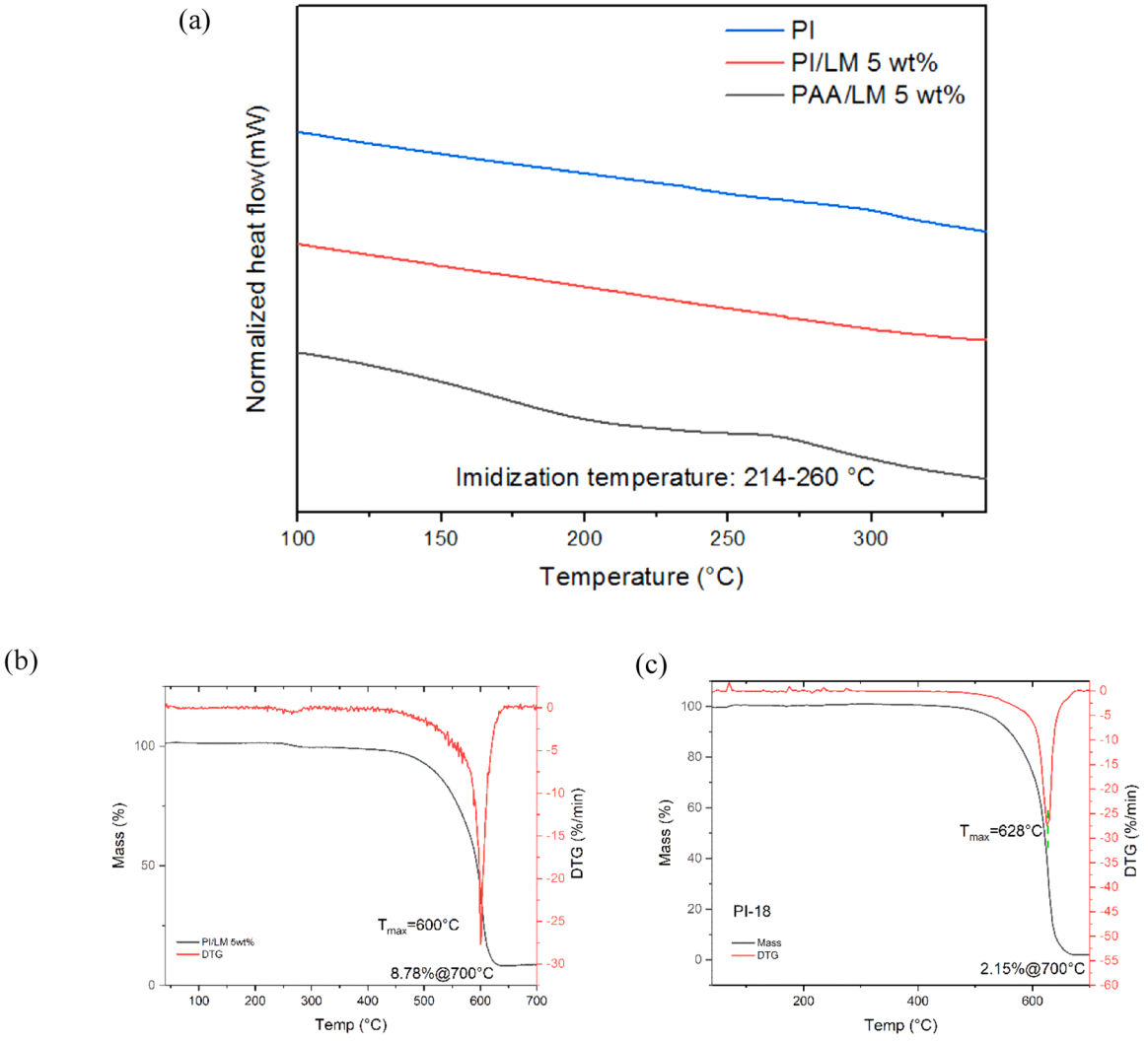

Fig. 7. Thermal characterization of pristine PI and PI/LM nanofibers: (a) DSC thermograms of PI, PI/LM (5 wt%), and PAA/LM precursor fibers; (b) TGA/DTG curves of PI/LM (5 wt%) nanofibers; (c) TGA/DTG curves of pristine PI nanofibers (PI−18).

nanospheres influenced the intrinsic thermal robustness of the polyimide (PI) matrix. Differential scanning calorimetry (DSC) was first employed to compare pristine PI, PI/LM (5 wt%), and precursor PAA/LM nanofibers. The DSC thermograms are presented in Fig. 7a. The precursor PAA/LM sample exhibited a clear thermal transition associated with the imidization process, whereas fully imidized PI-based membranes showed comparatively stable thermal profiles over the examined temperature range. These observations confirm the successful conversion of the electrospun precursor fibers into thermally stable PI nanofibers.

The imidization transition was observed within the approximate temperature range of 214–260 °C, which is consistent with thermal cyclization and solvent removal commonly reported for polyimide precursor systems. Importantly, the presence of LM did not introduce any abnormal thermal events or significant shift in the overall DSC behaviour of the PI membrane, indicating that moderate LM incorporation did not interfere with the formation or thermal integrity of the imide structure.

Thermogravimetric analysis (TGA) and derivative thermogravimetry (DTG) were further conducted to assess high-temperature decomposition behaviour. As shown in Fig. 7b, the PI/LM (5 wt%) nanofiber membrane exhibited a maximum decomposition temperature (Tmax) of approximately 600 °C, demonstrating excellent thermal resistance suitable for elevated-temperature applications. Residual mass at 700 °C was measured at 8.78%, indicating the presence of thermally stable inorganic or metallic residue associated with LM incorporation.

For comparison, the pristine PI membrane (PI−18) showed a slightly higher Tmax of approximately 628 °C, together with a lower residual mass of 2.15% at 700 °C, as presented in Fig. 7c. The modest reduction in Tmax after LM addition suggests that incorporation of dispersed LM nanospheres may slightly influence the thermal decomposition pathway of the polymer matrix, possibly through local heat-transfer effects or disruption of chain packing at the filler-matrix interface. Nevertheless, the decomposition temperature of the composite remained exceptionally high, confirming that the PI/LM membrane retained the outstanding thermal resistance characteristic of polyimide.

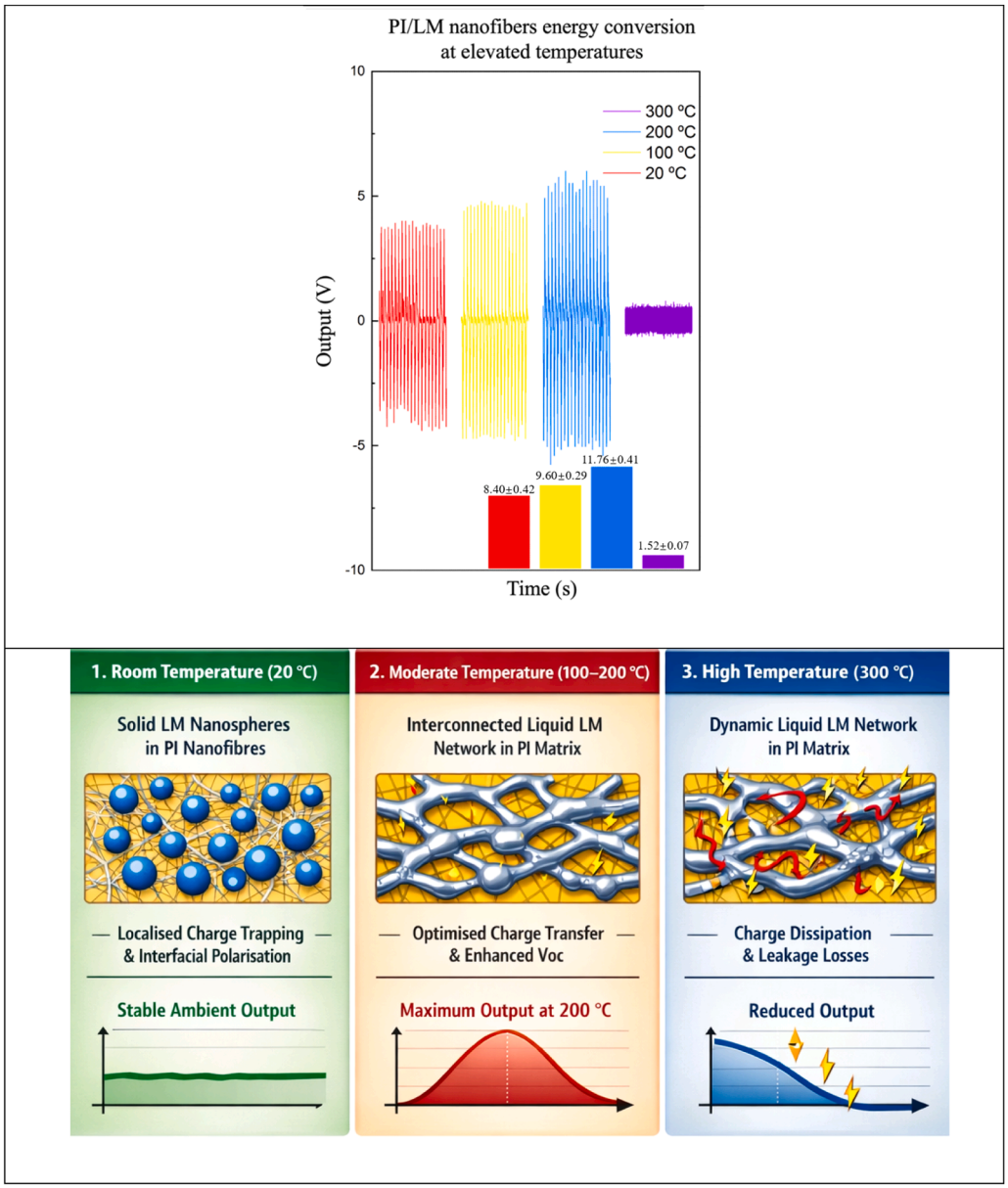

Fig. 8. Open-circuit voltage (Voc) output of the optimised PI/LM nanofiber membrane (5 wt% LM) measured at different operating temperatures (20, 100, 200, and 300 °C), showing maximum performance at 200 °C. and Proposed mechanism of the effect at different temperatures.

The higher char/residual content observed for the PI/LM membrane is reasonably attributed to the non-volatile metallic component of the composite, which remains stable over the examined temperature range. This increased residue does not indicate inferior performance; rather, it reflects the presence of LM domains that do not undergo polymer-like thermal degradation.

These findings demonstrate that the incorporation of 5 wt% LM does not compromise the key thermal advantages of the PI nanofiber platform. The composite membrane maintains high thermal stability while simultaneously providing enhanced triboelectric performance, making it a suitable candidate for operation under harsh or elevated-temperature environments.

3.5. Elevated-temperature triboelectric performance

To evaluate the suitability of the PI/LM nanofiber membrane for harsh-environment energy harvesting, the triboelectric output performance of the optimised 5 wt% LM sample was investigated under elevated temperatures. Open-circuit voltage (Voc) measurements recorded at different operating temperatures are presented in Fig. 8. The PI/LM membrane exhibited a clear temperature-dependent response, indicating that thermal conditions strongly influence charge generation and retention within the triboelectric system.

At room temperature (20 °C), the membrane generated a Voc of 8.40 ±0.42 V. Increasing the operating temperature to 100 °C enhanced the output to 9.60±0.29 V, while a further increase to 200 °C produced the maximum Voc of 11.76±0.41 V, corresponding to an improvement of approximately 40% relative to room-temperature operation. This trend suggests that moderate heating can beneficially activate triboelectric processes within the PI/LM dielectric layer. Enhanced dipolar mobility, increased interfacial polarization, and thermally assisted charge transfer at the contact interface may collectively contribute to the improved voltage generation observed at intermediate temperatures.

When the temperature was further increased to 300 °C, the output voltage decreased sharply to 1.52±0.07 V. The substantial decline at this temperature indicates that excessive heating introduces dominant charge-loss mechanisms that outweigh the beneficial polarization effects observed at lower temperatures. At sufficiently high temperature, accelerated charge dissipation, increased thermionic emission, reduced surface charge retention, and thermally induced leakage pathways may significantly suppress triboelectric performance.

The non-monotonic behaviour observed experimentally in Fig. 8 may reflect a competition between two temperature-dependent phenomena: (i) thermal activation of polarization and charge transfer, which enhances output at moderate temperatures, and (ii) temperature-induced charge decay, which dominates under more severe heating conditions. The optimum response at 200 °C suggests that the PI/LM membrane is suggested to maintain favourable dielectric behaviour within this intermediate operating window. A proposed temperature-dependent triboelectric behaviour, based on the experimental observations and plausible physical interpretation, is summarised in Table 2. At moderate temperatures, enhanced interfacial polarization and thermally activated charge transfer contribute positively to triboelectric output, whereas excessive heating promotes accelerated charge dissipation and reduced surface charge retention.

Compared with previously reported pristine PI systems, the relative enhancement in high-temperature output after LM incorporation was more moderate than the large gains observed under ambient conditions. This behaviour may be associated with the intrinsic thermal conductivity of gallium-based LM domains, which can facilitate faster heat transfer through the dielectric layer. As a result, localized temperature rise within the composite may be more pronounced than in pristine PI, accelerating thermally driven charge relaxation processes at elevated temperatures. While LM inclusions remain beneficial for ambient and moderate-temperature performance, their presence may partially limit output retention under extreme thermal exposure.

Table 2
Proposed temperature-dependent triboelectric mechanism of PI/LM nanofiber membranes.

Operating Condition	LM Behaviour	Triboelectric Effect	Resulting Output Behaviour
Room temperature (20 °C)	LM exists as well-dispersed nanospheres within PI nanofibers	Localized charge trapping and interfacial polarization	Stable ambient triboelectric output
Moderate temperature (100−200 °C)	**Proposed increase in** dipolar activity and interfacial polarization. Interconnected liquid channel.	Enhanced charge transfer and polarization response	Increased Voc with maximum output at 200 °C
High temperature (300 °C)	Increased thermal mobility and charge relaxation. **Possible local rearrangement of LM domains under elevated temperatures**	Accelerated charge dissipation and reduced surface charge retention	Significant reduction in triboelectric output

Nevertheless, the PI/LM membrane still delivered stable and measurable electrical output up to 300 °C, highlighting the robustness of the PI nanofiber platform and the ability of the composite membrane to function under demanding thermal conditions. The combination of strong room-temperature performance and retained operation at elevated temperature makes this material system attractive for self-powered sensing and energy harvesting in industrial or high-temperature environments.

These results suggest that controlled LM incorporation can enhance triboelectric performance while preserving the exceptional thermal operating window of PI nanofibers. An optimum operating temperature of 200 °C was identified for the investigated composite system.

3.6. Comparison with reported LM-based TENG systems

To highlight the distinctive characteristics of this work, the overall performance of the PI/LM nanofiber membrane was compared with representative literature data on LM-based TENGs. As summarized in Table 3, most previously reported LM-enabled TENGs have focused on flexible room-temperature devices for wearable sensing or high-output ambient energy harvesting, typically using fluoropolymer or elastomeric matrices. In contrast, the present study introduces a thermally robust electrospun polyimide (PI) nanofiber platform that combines LM-enabled triboelectric enhancement with operation under elevated temperatures up to 300 °C.

Although several LM-based systems report higher room-temperature output voltages, direct comparison of absolute voltage values should be interpreted cautiously because triboelectric performance is strongly dependent on device geometry, contact area, excitation force, frequency, counter tribomaterial, and measurement conditions. Accordingly, the key contribution of the present study is not solely peak voltage generation, but the development of an LM-integrated dielectric membrane capable of maintaining triboelectric functionality under harsh thermal environments.

The PI/LM membrane developed in this work achieved a room-temperature Voc of 8.40±0.42 V, increasing to 11.76±0.41 V at 200 °C, while retaining measurable output at 300 °C. To the best of current knowledge, few LM-based electrospun TENG systems have explicitly demonstrated such a broad elevated-temperature operating window. This highlights the advantage of combining the intrinsic thermal resistance of PI with the dielectric/interfacial benefits introduced by dispersed LM nanospheres.

In addition, the present work employed AFM/KPFM analysis to show that LM incorporation modifies the local surface electrostatic landscape

Table 3
Comparison of representative liquid metal-based triboelectric nanogenerator systems.

Ref.	Active Material/ Matrix	LM Type	Reported Output*	Applied Force	Operating Temperature	Key Feature
[19]	Electrospun PVDF-HFP nanofibers	Galinstan nanodroplets	Voc ≈ 1680 V; 24 W m^{-2}	1000 N,1−5 Hz	Room temperature	High-output flexible TENG
[20]	Surface-modified polymer composite	LM nanocapsules	Voc enhanced 4.0 × ; Power density 28.3 ×	10 N, 3 Hz	Room temperature	Wearable self-powered sensing
[28]	Sponge-type elastomer composite	LM droplets	Motion-sensing output	100 N/3 Hz	Room temperature	Omnidirectional flexible sensor
[29]	LM-modified all-nanofiber TENG	LM inner-encapsulated	Voc = 162 V; 176 mW m^{-2}	30 N/2 Hz	Room temperature	All-nanofiber multifunctional
[30]	3D-printed LM-elastomer composite	EGaIn-based	Ultra-high output (record values in printed LM-TENGs)	40 N/5 Hz	Room temperature	Extremely stretchable 3D-printed TENG
This work	Electrospun PI nanofibers	Gallium-based LM nanospheres	Voc = 8.40±0.42 V (20 °C); 11.76 ±0.41 V (200 °C); 1.52±0.07 V (300 °C)	10 N/2 Hz	Up to 300 °C	High-temperature operable LM-TENG

* **Note:** Absolute output values are highly dependent on device configuration, contact force, frequency, counter tribomaterial, and measurement conditions. The present work emphasizes thermal stability and high-temperature functionality.

of the nanofiber membrane, providing nanoscale evidence for a mechanism involving enhanced polarization and charge trapping. Such structure–property correlation further distinguishes the current study from many previous LM-based reports focused primarily on output metrics.

The present PI/LM nanofiber membrane extends the application scope of LM-based triboelectric materials beyond ambient-condition flexible electronics and establishes a practical route toward multifunctional TENG systems for high-temperature sensing and energy harvesting.

4. Conclusion

In this study, LM nanospheres were successfully incorporated into electrospun PI nanofibers to develop a triboelectric material capable of enhanced energy harvesting under elevated-temperature conditions. A sonication-assisted dispersion approach enabled stable integration of LM within the PI matrix, while preserving the continuous nanofibrous structure of the membrane. The experimental results demonstrate that LM incorporation improves the triboelectric performance of PI nanofibers. Based on the combined morphological, KPFM, and electrical characterization, the performance enhancement is proposed to be associated with enhanced interfacial polarization and localized charge trapping, although direct verification requires further dielectric and charge-decay analyses.

Among the investigated formulations, the membrane containing 5 wt% LM exhibited the best overall performance, delivering an open-circuit voltage of 8.40±0.42 V under ambient conditions together with improved capacitor charging behaviour and stable operation over 10,000 cycles. These results indicate that moderate LM incorporation can significantly improve triboelectric output without compromising structural durability.

Thermal characterization further showed that the PI/LM membrane retained the excellent heat resistance associated with polyimide, with a decomposition temperature near 600 °C. Under elevated-temperature testing, the triboelectric response increased with temperature and reached a maximum output of 11.76±0.41 V at 200 °C, before declining at more severe heating conditions due to dominant charge-loss processes. Importantly, measurable electrical output was still maintained at 300 °C, demonstrating the robustness of the composite membrane under harsh environments.

This work shows that combining thermally stable PI nanofibers with functional LM nanospheres provides an effective route for extending triboelectric nanogenerator technology beyond conventional room-temperature flexible systems. The developed PI/LM platform offers promise for self-powered sensing, waste-heat-adjacent monitoring, and mechanical energy harvesting in industrial environments where conventional polymer-based TENG materials are limited. Future studies may focus on optimizing LM particle size and loading, tailoring fiber architecture, and integrating the membranes into practical device designs for long-term operation in real high-temperature applications.

CRediT authorship contribution statement

Minoo Naebe: Writing – review & editing, Supervision, Resources, Funding acquisition, Conceptualization. **Prasaanth Ravi Anusuyadevi:** Writing – original draft, Visualization, Methodology, Formal analysis. **Peyman Taheri:** Writing – original draft, Resources, Investigation, Formal analysis. **Nauman Ali Choudhry:** Writing – original draft, Visualization, Investigation. **Agnieszka Kooijman:** Writing – original draft, Formal analysis, Data curation. **İlhan Özen:** Writing – original draft, Investigation, Formal analysis. **Peng Wu:** Writing – review & editing, Writing – original draft, Methodology, Investigation, Formal analysis. **Kamyar Shirvanimoghaddam:** Writing – original draft, Validation, Supervision, Methodology, Conceptualization.

Declaration of Competing Interest

The authors declare that they have no known competing financial interests or personal relationships that could have appeared to influence the work reported in this paper.

Appendix A. Supporting information

Supplementary data associated with this article can be found in the online version at doi:10.1016/j.materresbull.2026.114397.

Data availability

The data that has been used is confidential.

References

[1] D. Choi, Y. Lee, Z.-H. Lin, S. Cho, M. Kim, C.K. Ao, S. Soh, C. Sohn, C.K. Jeong, J. Lee, M. Lee, S. Lee, J. Ryu, P. Parashar, Y. Cho, J. Ahn, I.-D. Kim, F. Jiang, P. S. Lee, G. Khandelwal, S.-J. Kim, H.S. Kim, H.-C. Song, M. Kim, J. Nah, W. Kim, H. G. Menge, Y.T. Park, W. Xu, J. Hao, H. Park, J.-H. Lee, D.-M. Lee, S.-W. Kim, J. Y. Park, H. Zhang, Y. Zi, R. Guo, J. Cheng, Z. Yang, Y. Xie, S. Lee, J. Chung, I.-K. Oh, J.-S. Kim, T. Cheng, Q. Gao, G. Cheng, G. Gu, M. Shim, J. Jung, C. Yun, C. Zhang, G. Liu, Y. Chen, S. Kim, X. Chen, J. Hu, X. Pu, Z.H. Guo, X. Wang, J. Chen, X. Xiao, X. Xie, M. Jarin, H. Zhang, Y.-C. Lai, T. He, H. Kim, I. Park, J. Ahn, N.D. Huynh, Y. Yang, Z.L. Wang, J.M. Baik, D. Choi, Recent advances in triboelectric nanogenerators: from technological progress to commercial applications, ACS Nano 17 (2023) 11087–11219, https://doi.org/10.1021/acsnano.2c12458.
[2] X. Pu, C. Zhang, Z.L. Wang, Triboelectric nanogenerators as wearable power sources and self-powered sensors, Natl. Sci. Rev. 10 (2023) nwac170.
[3] D. Tao, P. Su, A. Chen, D. Gu, M. Eginligil, W. Huang, Electro-spun nanofibers-based triboelectric nanogenerators in wearable electronics: status and perspectives, npj Flex. Electron. 9 (2025) 4, https://doi.org/10.1038/s41528-024-00357-5.

[4] Z. Li, Y. Lu, X. Wang, T. Li, Y. Xiao, Y. Li, W. Kang, All-weather triboelectric nanogenerator with bidirectional temperature regulation and hydrophobicity for energy harvesting and motion detection, Chem. Eng. J. 522 (2025) 168011, https://doi.org/10.1016/j.cej.2025.168011.
[5] S. Velmurugan, T.V.R. Murugan, Optimization of drilling parameters for Spanish cherry fiber reinforced hybrid composites using Taguchi analysis, Int. J. Comput. Exp. Sci. Eng. 11 (2025), https://doi.org/10.22399/ijcesen.3978.
[6] D.R.G. Kabo, M. Tumpu, D.B. Pinasang, C. Kandou, H. Tumengkol, H.-P. Lee, Enhancing the performance and sustainability of lightweight hebel bricks using local Coco fiber additives: a green material innovation for circular construction, Int. J. Comput. Exp. Sci. Eng. 12 (2026), https://doi.org/10.22399/ijcesen.4490.
[7] H. Khelaifa, H. Chaib, A. Hima, A. Khelaifa, Sustainable rehabilitation of oil-contaminated sand: enhancing mechanical properties through alluvial sand substitution and polypropylene fiber reinforcement, Int. J. Comput. Exp. Sci. Eng. 12 (2026), https://doi.org/10.22399/ijcesen.4986.
[8] A.K. Jawad, I.M. Ali, M.K. Abed, I.A. Saeed, M.S. Nasr, T.M. Hashim, Flexural behavior of blended slurry-infiltrated fibrous concrete boards made with hybrid fibers and nano slag, Int. J. Comput. Exp. Sci. Eng. 11 (2025), https://doi.org/10.22399/ijcesen.1749.
[9] T. Zhao, J. Gao, Y. Zheng, J. Liu, Y. Ni, W. Zhao, Q. Guan, Z. You, High-temperature enhancing triboelectric nanogenerator based on antioxidant liquid crystalline polyarylate, Adv. Mater. 37 (2025) 2510431, https://doi.org/10.1002/adma.202510431.
[10] Z. Chen, W. Xia, R. Ming, M. Hao, Z. Du, B. Zhou, S. Yang, Y. Song, J. Wang, X. Yin, High-temperature stable aramid nanofibers-based triboelectric nanogenerators with regeneratability and designability for real hot environments monitoring, Nano Energy 136 (2025) 110772, https://doi.org/10.1016/j.nanoen.2025.110772.
[11] C. Xu, A.C. Wang, H. Zou, B. Zhang, C. Zhang, Y. Zi, L. Pan, P. Wang, P. Feng, Z. Lin, Z.L. Wang, Raising the working temperature of a triboelectric nanogenerator by quenching down electron thermionic emission in contact-electrification, Adv. Mater. 30 (2018) 1803968, https://doi.org/10.1002/adma.201803968.
[12] C. Wang, H. Guo, P. Wang, J. Li, Y. Sun, D. Zhang, An advanced strategy to enhance TENG output: reducing triboelectric charge decay, Adv. Mater. 35 (2023) 2209895, https://doi.org/10.1002/adma.202209895.
[13] F. Shi, X. Wei, H. Wang, X. Wu, Electrospun polyimide nanofiber-based triboelectric nanogenerator for harvesting energy at elevated temperatures, ACS Appl. Electron. Mater. 4 (2022) 4569–4575, https://doi.org/10.1021/acsaelm.2c00781.
[14] P. Wu, K. Shirvanimoghaddam, R.T. Leon, Ir Prasaanth Ravi Anusuyadevi, P. Taheri, P. Gonugunta, A.V. Ellis, M. Naebe, Beyond the limits: pushing the boundaries of polyimide triboelectric nanogenerator performance at elevated temperatures, Chem. Eng. J. 512 (2025) 161809, https://doi.org/10.1016/j.cej.2025.161809.
[15] B.Y. Kim, W.Y.W. Yusoff, P. Matteini, P. Baumli, B. Hwang, Recent advances in liquid metal-based stretchable and conductive composites for wearable sensor applications, Biosensors 15 (2025) 466, https://doi.org/10.3390/bios15070466.
[16] F.-C. Liang, B.C.K. Tee, Functional liquid metal polymeric composites: fundamentals and applications in soft wearable electronics, Adv. Funct. Mater. 34 (2024) 2400284, https://doi.org/10.1002/adfm.202400284.
[17] S. Oh, Y. Lee, J. Yang, Y. Lee, S. Won, S.S. Han, J.H. Kim, T. Lim, Liquid metal particles–graphene core–shell structure enabled hydrogel-based triboelectric nanogenerators, Gels 12 (2026) 86, https://doi.org/10.3390/gels12010086.
[18] Z. Li, B. Xu, J. Han, D. Tan, J. Huang, Y. Gao, H. Fu, Surface-modified liquid metal nanocapsules derived multiple triboelectric composites for efficient energy harvesting and wearable self-powered sensing, Chem. Eng. J. 460 (2023) 141737, https://doi.org/10.1016/j.cej.2023.141737.
[19] Z. Sha, C. Boyer, G. Li, Y. Yu, F.-M. Allioux, K. Kalantar-Zadeh, C.-H. Wang, J. Zhang, Electrospun liquid metal/PVDF-HFP nanofiber membranes with exceptional triboelectric performance, Nano Energy 92 (2022) 106713, https://doi.org/10.1016/j.nanoen.2021.106713.
[20] Z. Li, B. Xu, J. Han, D. Tan, J. Huang, Y. Gao, H. Fu, Surface-modified liquid metal nanocapsules derived multiple triboelectric composites for efficient energy harvesting and wearable self-powered sensing, Chem. Eng. J. 460 (2023) 141737, https://doi.org/10.1016/j.cej.2023.141737.
[21] K. Shirvanimoghaddam, P. Wu, I. Ozen, N.A. Choudhry, M. Naebe, Energizing change: liquid-metal-enabled nanogenerators for smart textiles, Small Struct. 7 (2026) e202500886, https://doi.org/10.1002/sstr.202500886.
[22] A. Hajalilou, E. Parvini, C. Majidi, Sustainable liquid metal composites for soft electronics and e-waste reduction, Adv. Mater. 38 (2026) e12968, https://doi.org/10.1002/adma.202512968.
[23] H. Hwang, H. Lee, J. Baek, H. Kang, Y. Kim, Engineering liquid metal particles: design rules for sonication-based methods, Nano Lett. 25 (2025) 9881–9890, https://doi.org/10.1021/acs.nanolett.5c00692.
[24] Q. Wu, Z. Ma, C. Wang, Y. Tao, S. Wang, Z. Jin, T. Gao, C. Li, P. Liu, Carbon nanofibers with small-sized Co nanoparticles and structural defects via a confined-coordination growth strategy toward electromagnetic wave absorption, J. Adv. Ceram. 14 (2025) 9221210, https://doi.org/10.26599/JAC.2025.9221210.
[25] P. Liu, Z. He, X. Li, L. Ding, S. Liu, J. Kong, Multifunctional hollow carbon microspheres enable superior electromagnetic wave response and corrosion barrier, Adv. Mater. 37 (2025) 2500646, https://doi.org/10.1002/adma.202500646.
[26] W. Geng, P. Liu, Hollow Zn1-xCo2-yNixFeyO4 spinel via multi-metal ion doping: ultralight and broadband microwave absorber (N/A-N/A), Soft Sci. 6 (2026), https://doi.org/10.20517/ss.2025.113.
[27] Z. He, H. Xu, L. Shi, X. Ren, J. Kong, P. Liu, Hierarchical Co2P/CoS2@C@MoS2 composites with hollow cavity and multiple phases toward wideband electromagnetic wave absorption, Small 20 (2024) 2306253, https://doi.org/10.1002/smll.202306253.
[28] J. Park, I. Kim, J. Yun, D. Kim, Liquid-metal embedded sponge-typed triboelectric nanogenerator for omnidirectionally detectable self-powered motion sensor, Nano Energy 89 (2021) 106442, https://doi.org/10.1016/j.nanoen.2021.106442.
[29] L. Yang, W. Hu, R. Cao, Q. Zhou, C. Hu, B. Dong, H. Song, L. Xu, Liquid metal modified all-nanofiber triboelectric nanogenerator for energy harvesting and multi-functional self-powered sensing, Chem. Eng. J. 517 (2025) 164372, https://doi.org/10.1016/j.cej.2025.164372.
[30] K. Parida, G. Thangavel, G. Cai, X. Zhou, S. Park, J. Xiong, P.S. Lee, Extremely stretchable and self-healing conductor based on thermoplastic elastomer for all-three-dimensional printed triboelectric nanogenerator, Nat. Commun. 10 (2019) 2158, https://doi.org/10.1038/s41467-019-10061-y.